

Failure characteristics of combined coal-rock with different interfacial angles

Tong-Bin Zhao^{1,2}, Wei-Yao Guo^{*2}, Cai-Ping Lu³ and Guang-Ming Zhao¹

¹Key Laboratory of Safety and High-efficiency Coal Mining, Ministry of Education
(Anhui University of Science and Technology), Huainan, Anhui, 232001, P.R. China

²State Key Laboratory of Mining Disaster Prevention and Control

Co-founded by Shandong Province and the Ministry of Science and Technology,
Shandong University of Science and Technology, Qingdao, Shandong 266590, P.R. China

³School of Mining Engineering, Key Laboratory of Deep Coal Resource Mining (Ministry of Education),
China University of Mining and Technology, Xuzhou, Jiangsu 221116, P.R. China

(Received November 25, 2015, Revised April 30, 2016, Accepted May 10, 2016)

Abstract. In order to investigate the influence of the interfacial angle on failure characteristics and mechanism of combined coal-rock mass, 35 uniaxial/biaxial compressive simulation tests with 5 different interfacial angles of combined coal-rock samples were conducted by PFC2D software. The following conclusions are drawn: (1) The compressive strength and cohesion decrease with the increase of interfacial angle, which is defined as the angle between structure plane and the exterior normal of maximum principal plane, while the changes of elastic modulus and internal friction angle are not obvious; (2) The impact energy index K_E decreases with the increase of interfacial angle, and the slip failure of the interface can be predicted based on whether the number of acoustic emission (AE) hits has multiple peaks or not; (3) There are four typical failure patterns for combined coal-rock samples including I (V-shaped shear failure of coal), II (single-fracture shear failure of coal), III (shear failure of rock and coal), and IV (slip rupture of interface); and (4) A positive correlation between interfacial angle and interface effect is shown obviously, and the interfacial angle can be divided into weak-influencing scope (0-15°), moderate-influencing scope (15-45°), and strong-influencing scope (> 45°), respectively. However, the confining pressure has a certain constraint effect on the interface effect.

Keywords: particle flow; combined coal-rock; interfacial angle; failure pattern; mechanical properties

1. Introduction

The geotechnical properties of rock associated with coal seams play a significant role in the design, operation, and safety of underground and open-cut mining operations (Ward 1984, Thomas 2002). Specifically the combined structure composed of coal and rock mass, and its mechanical behavior reflects the combination of coal, rock and interface at different loading mechanism. Instability may directly reflect the dynamic disaster, such as roof fall, coal bump, and rockburst. The nature of coal-rock itself, referred to as coal-rock substance, dominates in the geo-mechanical behavior, and extensive geo-mechanical tests have been conducted to evaluate its geotechnical properties (Brady and Brown 1993, Bell 2000, Chen *et al.* 2012). It is noted here that the

*Corresponding author, Ph.D. Student, E-mail: 363216782@qq.com

parameters of mechanical discontinuities, such as joints, faults and bedding planes (interface) may also be influential on stability of combined coal-rock mass. A comprehensive understanding of deformation and failure characteristics of combined coal-rock mass is therefore essential in assessing the potential dynamic hazard before, during and after the mining process.

In the process of deep coal resources exploitation, the engineering accidents and disasters often occur due to the instability and failure of coal and rock structure. It is known that coal-rock dynamic disasters can be easily induced when roof and floor suddenly lose stability in the process of coal mining (Lu *et al.* 2015, Tan *et al.* 2015). Therefore, the interaction between the surrounding rock and coal is a key influencing factor to keep the dynamic equilibrium of structure of roof, unmined coal block and floor. In recent years, many researches focused on combined coal-rock structure have been conducted, and some outstanding achievements have been obtained and reported. For example, Petukhov and Linkov (1979) analyzed the stability of general bipartite system and the roof-coal system while studying the stable behavior of rock mass after post-peak point. Zuo *et al.* (2013) found that the failure of combined coal-rock mass mainly occurs within the coal, and the confining pressure, combination modes, and loading conditions play a very important role on its failure mode. Inmaculada Alvarez-Fernandez *et al.* (2013) analyzed the interaction between seam operations and associated fault rock by using numerical methods. Vakili and Hebblewhite (2010) developed a new cavability assessment criterion for top-coal in combined coal-rock system composed of immediate roof, top coal, cutting coal, and floor based on numerical modeling. Poulsen *et al.* (2014) studied the strength reduction of a coal pillar due to water saturation embedded in combined structure composed of roof, coal pillar and floor using numerical modeling. Mishra and Verma (2015) performed a series of uniaxial and triaxial creep tests on shale specimens in coal measure to investigate the deformation characteristics of roof rock with regards to time and failure mechanism under complex stress conditions. Mohtarami *et al.* (2014) studied the interaction between soil mass and downward rock blocks using a theoretical model for stability analysis.

Usually, both coal and surrounding rock mass are sedimentary and their stability is affected significantly by geological structures. According to the dip angle of coal seam, it can be divided into nearly horizontal, gently dip, dip, and steep dip coal seams. One of the main failure modes of coal and rock mass is shear-slip along the interface between coal and rock mass. Thus, the interface angle has a significant influence on the mechanical behavior of combined coal-rock mass. Unfortunately, only few literatures attempted to clarify the above-mentioned issue. Even with the limited study, the failure characteristics and AE effects were not further analyzed. For example, Zhao *et al.* (2015a) analyzed the effects of interface cohesive strength, rock thickness and stress level on failure of combined coal-rock by mechanical and experimental methods. Guo *et al.* (2011) experimentally investigated the mechanism of macroscopic deformation and failure of combined coal-rock samples with different interfacial angle.

The method of particle flow simulation can effectively reflect microstructure characteristics and essentially reveal the mechanism of coal and rock deformation and failure regime. In this paper, comprehensive uniaxial and biaxial compressive simulation tests of combined coal-rock samples with different interfacial angle were conducted by PFC2D software, and the essence is to interpret the influencing mechanism of the interfacial angle on strength, energy release, and AE characteristics of combined coal-rock mass, furthermore, to reveal its failure mechanism. The work is expected to provide some references to clarify the mechanical properties and the instability failure mechanism of combined coal-rock mass with different interfacial angle during the extraction process of coal resources.

2. Particle flow model of combined coal-rock samples

The bonding models of particle flow are divided into two patterns-contact and parallel forms. The contact model is commonly used to simulate particle materials such as soil, while the parallel model is used to simulate the compact materials such as coal and rock materials (Zhao *et al.* 2015b). Therefore, the parallel bond model was adopted in this paper. The parameters need to be set are friction coefficient (μ), bond stiffness (k_n and k_s), parallel bond stiffness (\bar{k}_n and \bar{k}_s), parallel bond strength (σ_n and σ_s), radius coefficient of parallel bond (λ). These parameters can be obtained from the Eq. (1) (Yin *et al.* 2015).

$$\begin{cases} k_n = 2E_c \\ k_s = \frac{k_n}{k_n/k_s} \\ \bar{k}_n = \frac{\bar{E}_c}{2r} \\ \bar{k}_s = \frac{\bar{k}_n}{k_n/k_s} \end{cases} \quad (1)$$

Where E_c and \bar{E}_c are the elastic modulus of grain contact and parallel grain contact, respectively; both (k_n/k_s) and (\bar{k}_n/\bar{k}_s) are generally to be set 2.5; r is the mean radius between two grains; λ is often to be set 1. Generally, E_c and \bar{E}_c are equal, σ_n and σ_s are equal, and the four parameters can be determined by the method of micro-mechanical parameters calibration.

Here, the parallel cylindrical model was established and was generated by radius extension method, and the diameter and height of the model are 50 mm and 100 mm, respectively. The loading rate was 0.01 mm/s. The model is shown in Fig. 1 and the micro-parameters of coal and rock mass are listed in Table 1. In order to analyze the effects of interfacial angle, the strength and height ratios of rock to coal were set to be 3:1 and 1:1, respectively. In total, 35 uniaxial and biaxial compressive simulation tests were performed with five interfacial angles of 0° , 15° , 30° , 45° , and 60° , respectively. The confining stress of biaxial tests was set to be 1 MPa, 5 MPa, 10 MPa, 15 MPa, 20 MPa, and 30 MPa, respectively.

The AE events can reflect the crack formation of rock (Tan *et al.* 2000, 2011). In the parallel

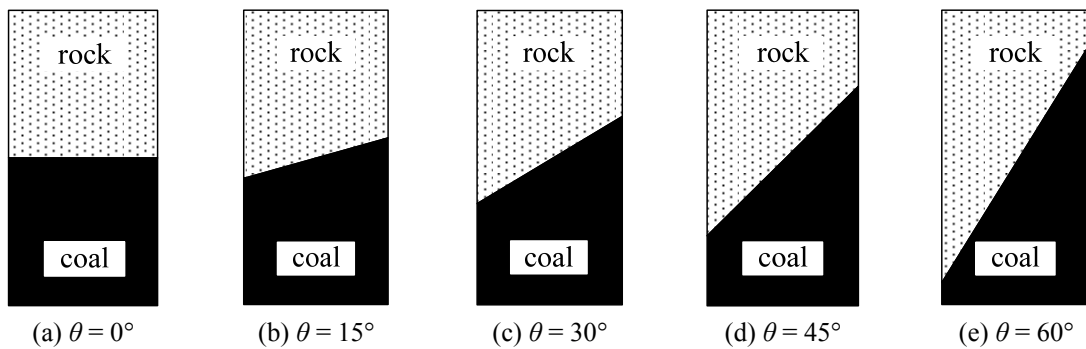


Fig. 1 Test models

Table 1 Micro-parameters of coal and rock

Materials	Density (/kg/m ³)	Radius /mm	Friction coefficient	Radius of parallel bond /mm	Elastic modulus /GPa	Bonding strength /MPa
Coal	1800	0.2-0.3	0.5	1	4	15
Rock	2600				12	45

bonding model of PFC2D, the development of each crack produce an AE pulse, and AE events of coal-rock failure can be simulated and calculated by recording the number of cracks and post-processing of data. During the process of uniaxial compressive tests, the time series characteristic curves of AE can be obtained by the method above to investigate the influencing mechanism of interfacial angle on AE characteristics of combined coal-rock mass.

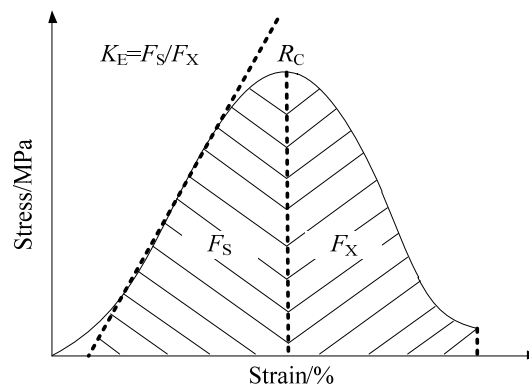
The change of deformation energy during the loading process of uniaxial compressive tests can be analyzed by the developed programming with built-in fish language in the uniaxial tests, and then the influence of interfacial angle on energy accumulation and release of combined coal-rock is revealed. The deformation energy E_C is calculated by Eq. (2).

$$E_C = \frac{1}{2} \sum_{N_C} (|F_i^n|^2 / k^n + |F_i^s|^2 / k^s) \quad (2)$$

where N_C is the number of contacts, $|F_i^n|$ and $|F_i^s|$ are the magnitudes of the normal and shear components of contact force, and k^n and k^s are the normal and shear-contact stiffness, respectively.

The impact energy index K_E , elastic energy index W_{ET} , and dynamic failure time D_T are often used for evaluating the rockburst tendency of coal. In this paper, the impact energy index K_E is introduced to study the effect of interfacial angle on the energy evolution of combined coal-rock mass. As shown in Fig. 2, the K_E refers to the ratio of the accumulative deformation energy F_s before peak stress to the releasable deformation energy F_x after peak stress under the condition of uniaxial compressive load. It reflects the energy transformation during the process of deformation and failure of coal-rock combination bodies. K_E is defined as the Eq. (3).

$$K_E = F_s / F_x \quad (3)$$

Fig. 2 Calculation Chart of K_E

where F_s is the accumulative deformation energy before peak stress and F_x is the releasable deformation energy after peak stress.

3. Simulation results and analysis

3.1 The influence of interfacial angle on strength characteristics of samples

Fig. 3 shows the stress-strain curves of uniaxial compressive tests of combined coal-rock samples. When the interfacial angles are 0° and 15° to the horizontal plane, the stress decreases rapidly after the peak. When this interfacial angle increases to 30° , the stress obviously manifests a short slip instead of sudden decrease after the peak. When the interfacial angles are 45° and 60° , such slip becomes more pronounced.

Fig. 4 shows the nonlinear relationship between the uniaxial compressive strength (UCS) and the interfacial angle. The fitting curve is expressed as $\sigma_c(\theta) = 18.7162 + 0.0117\theta - 0.00175\theta^2$. It is obviously indicated that the UCS firstly starts to decrease slowly and then reduce rapidly with the increase of interfacial angle. However, the elastic modulus almost does not vary along with the interfacial angle as shown in Fig. 3, which indicates that the stress-strain curves are coincident in

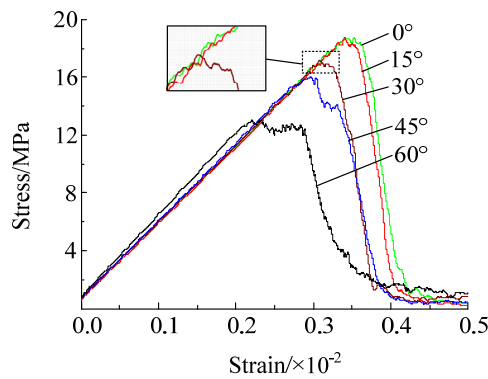


Fig. 3 Stress-strain curves of combined coal-rock under the uniaxial compressive load

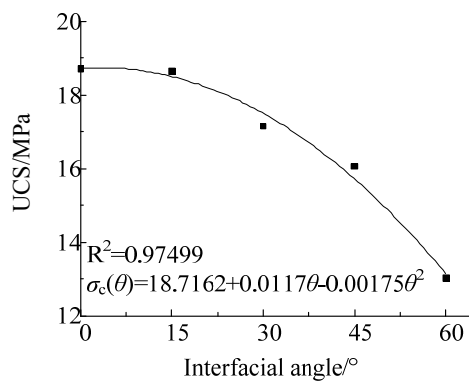


Fig. 4 Relationship between UCS and the interfacial angle

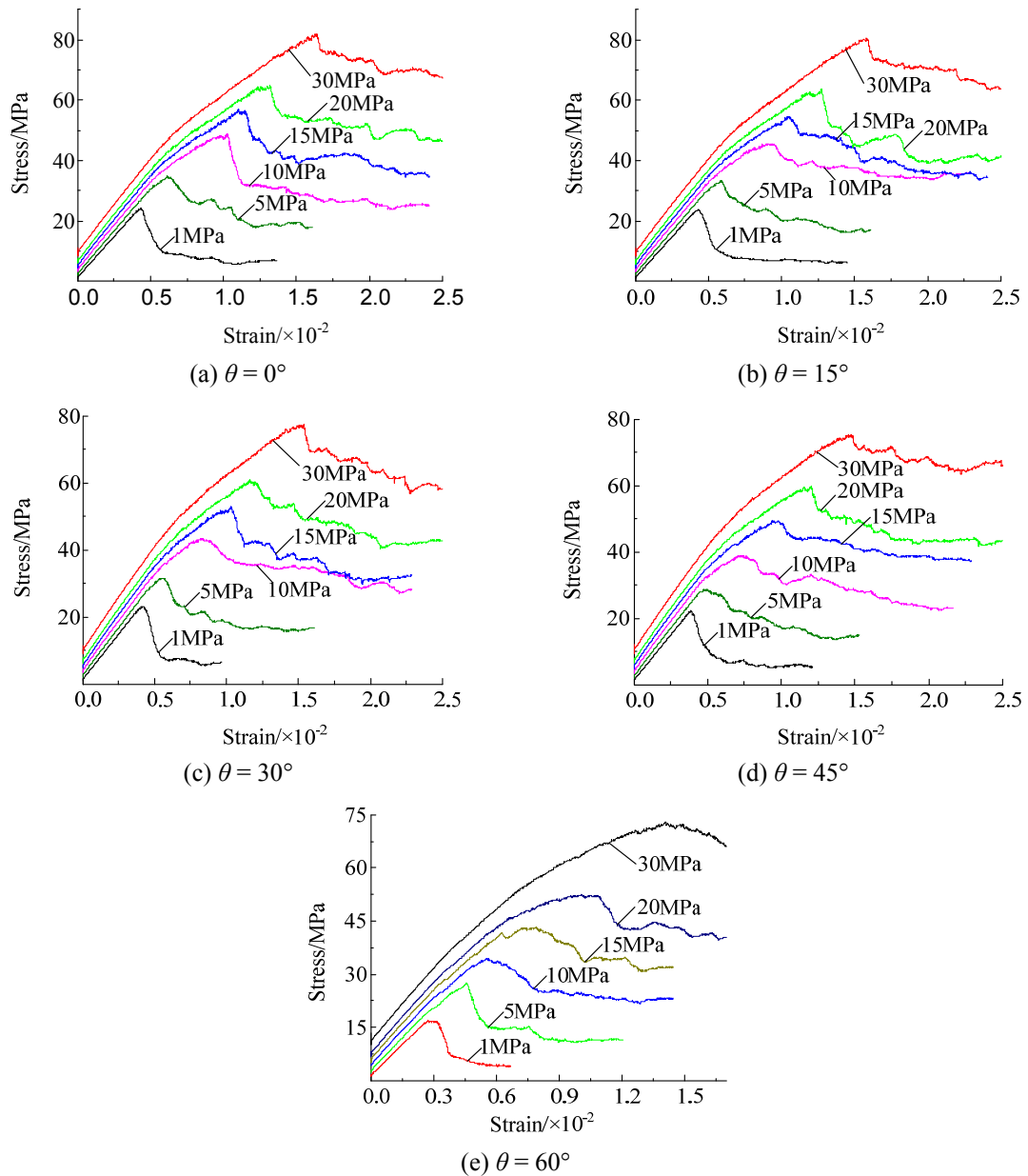


Fig. 5 Stress-strain curves of combined coal-rock samples under different confining pressure (Note: the confining pressure values in legend are 1 MPa, 5 MPa, 10 MPa, 15 MPa, 20 MPa, and 30 MPa, respectively)

the elastic deformation stage.

Fig. 5 shows the stress-strain curves of combined coal-rock samples with the interfacial angles of 0° , 15° , 30° , 45° , and 60° under different confining pressures. The samples show brittle failure under low confining stress. The brittle failure, however, turns into ductility failure under high confining stress, especially when the interfacial angle increases. This phenomenon is shown

clearly between the Figs. 5(a) and (e). Besides that, the failure strength decreases obviously with the increase of the interfacial angle.

Fig. 6 shows strength-confining pressure regression curves of combined coal-rock samples. It is indicated that failure strength of combined coal-rock samples increases linearly with the confining pressure. For instance, when the interfacial angle is 60°, the fitting curve is expressed as

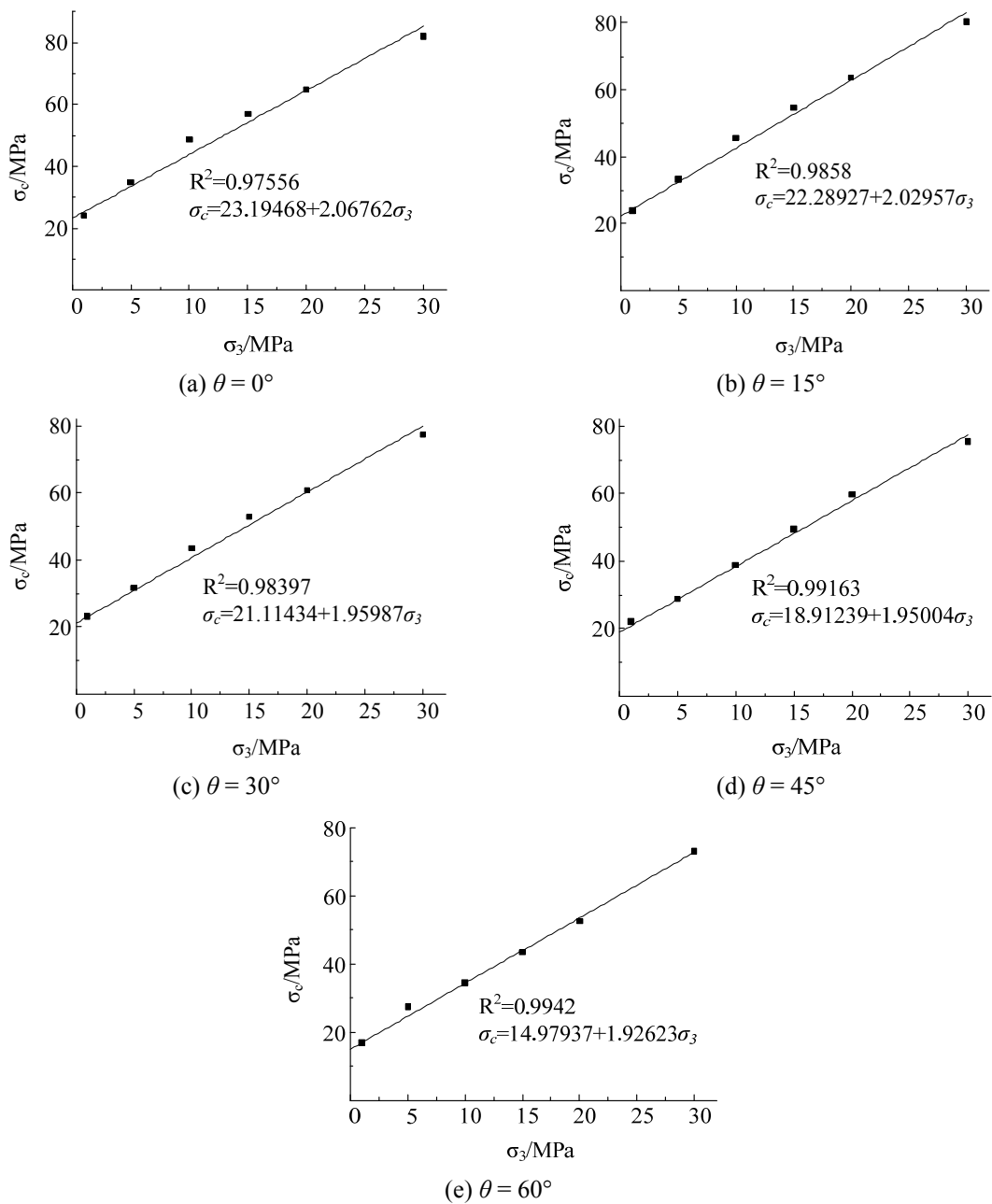


Fig. 6 Failure strength of combined coal-rock samples under different confining pressure

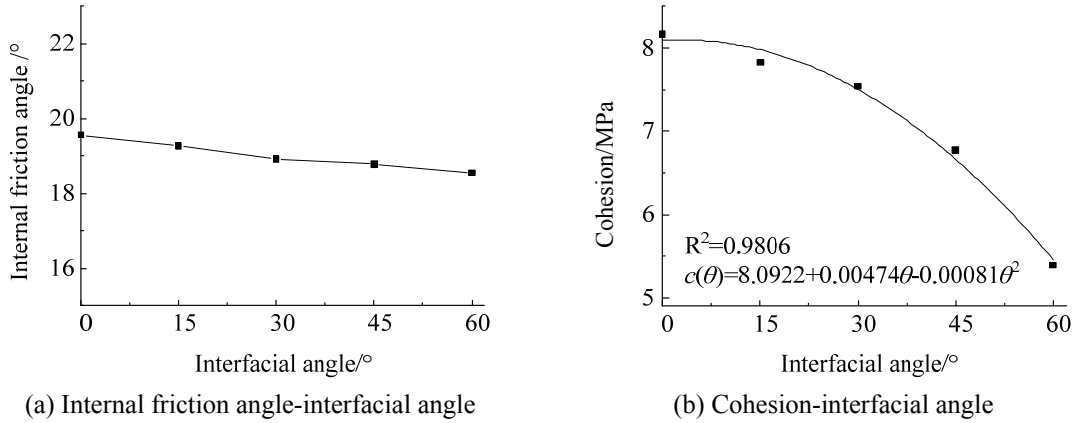


Fig. 7 Relationship between the internal friction angle, cohesion and interfacial angle

$\sigma_c = 14.97937 + 1.92623\sigma_3$ (σ_c and σ_3 represent the failure strength and the confining pressure, respectively). But, the increase rates of failure strength of combined coal-rock samples with regard to confining pressure at different interfacial angle are varied. If the confining stress is fixed, the compressive failure strength decreases with the increase of interfacial angle, while the decrease rate is opposite.

The relationship curves of internal friction angle, cohesion with regard to interfacial angle are shown in Fig. 7. The variation of internal friction angle is not obvious with the increase of interfacial angle, while cohesion gradually decreases. The nonlinear regression (the fitting curve is $c(\theta) = 8.0922 + 0.00474\theta - 0.00081\theta^2$) between cohesion and interfacial angle is presented.

3.2 The influence of interfacial angle on strain energy characteristics

Fig. 8 shows the strain energy-strain curves of combined coal-rock samples with different interfacial angle. Before peak stress, the strain energy firstly starts to increase slowly, and then quickly rises. Before the failure of samples, the smaller the interfacial angle is, the larger the accumulated strain energy is. The post-peak curves show that the smaller the interfacial angle is, the steeper the post-peak curve is, and the faster the release rate of strain energy is. With the

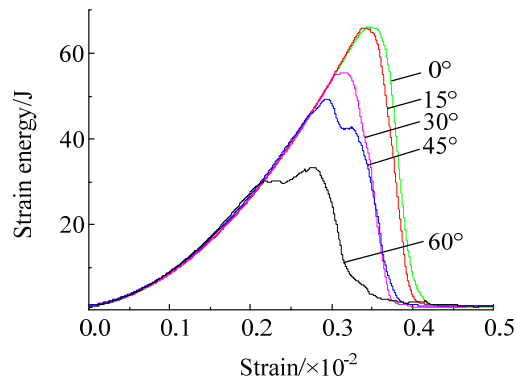


Fig. 8 Strain energy-strain curve

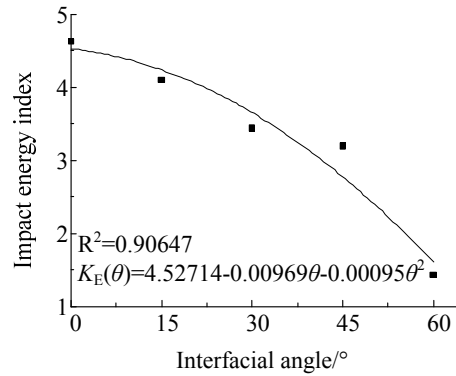


Fig. 9 Relationship between impact energy index and interfacial angle

gradual increase of interfacial angle, the strain energy curves obviously fluctuate near the peak of strain energy, especially when the interfacial angles are 45° and 60°, respectively.

Fig. 9 shows the relationship curves between impact energy index and interfacial angle. A nonlinear relation (the fitting curve is $K_E(\theta) = 4.52714 - 0.00969\theta - 0.00095\theta^2$) is presented.

Fig. 9 indicates that impact energy index decreases with the increase of interfacial angle, while the decrease rate is opposite. Two main reasons for interpretation are proposed: (1) With the increase of interfacial angle, the combined coal-rock shows a significant trend of reciprocal slip due to the interfacial effect, which causes the decrease of deformation and the corresponding strain energy; and (2) the uniaxial compressive strength decreases with increase of interfacial angle, while the elastic modulus does not obviously vary, which causes less energy accumulated at pre-peak stage of combined coal-rock deformation and failure. This indicates that the increase of interfacial angle cannot essentially cause the decrease of rockburst tendency of coal-rock for practical underground mining. On the contrary, the failure pattern of coal-rock mass mainly manifests the reciprocal slip with the increase of interfacial angle, which can trigger rockburst hazard more easily with significant characteristics of slip and instability due to the failure of interface.

3.3 The influence of interfacial angle on AE characteristics

Fig. 10 shows the stress and AE variation curves in the process of deformation and failure of combined coal-rock samples under the uniaxial compression.

Before peak stress, the stress-strain curve is almost linear, and the whole curve can be divided into four phases according to AE characteristics, which are (I) quiet period; (II) developing period, (III) booming period; and (IV) dropping period, respectively. AE characteristics at the quiet and dropping stages have no obvious link to the interfacial angle. When the interfacial angle is 60°, AE characterizes the very transient developing period, and AE almost quickly transits from quiet period to booming period in process of samples deformation and failure. In the booming period, when the interfacial angles are 0° and 15°, the number of AE hits has only one single peak. When the interfacial angle is 30°, the number of peak AE hits becomes two, which means that the interface has the obvious effect on the failure of combined coal-rock samples. When the interfacial angles are 45° and 60°, the number of AE hits continues to increase simultaneously accompanied with multiple abrupt drops during the slip period. Each drop of AE hits indicates a slip, and AE

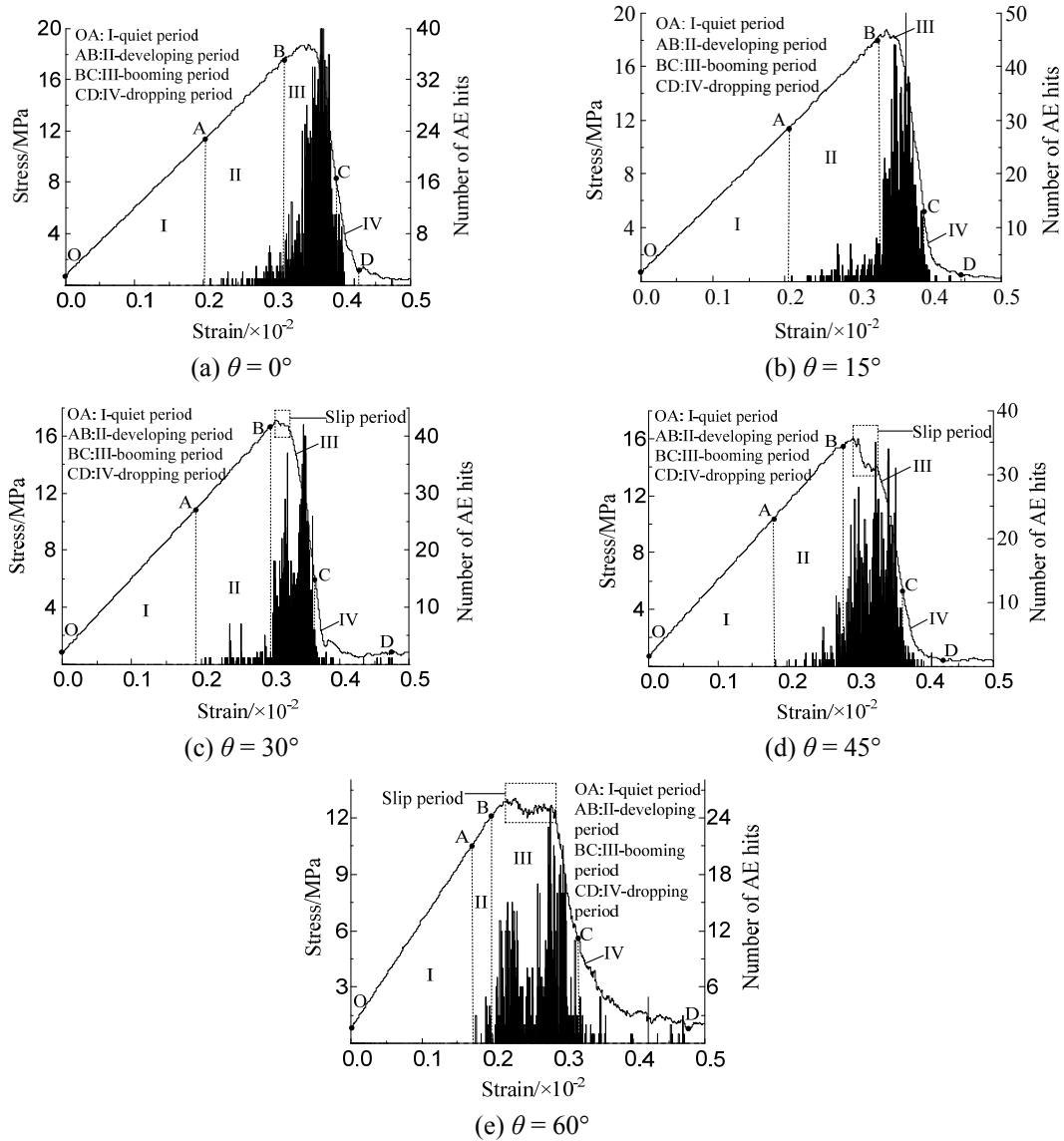


Fig. 10 Stress-strain and AE variation curves

reaches the maximum prior to the final failure after slip period, which fully confirms that the interface effect plays a major role on the deformation and failure of combined coal-rock samples.

Table 2 shows the statistical descriptions of AE characteristics of combined coal-rock samples with different interfacial angle deformation and failure.

According to Fig. 10 and Table 2, the slip fracture of combined coal-rock interface can be early predicted based on the precursory signs of AE. When the developing period of AE is transient as AE quickly transits from quiet period to booming period, the failure pattern of coal-rock is mainly due to slip fracture. When AE significantly fluctuates or the number of peak AE hits tends multiple, the slip failure of interface might have occurred. Therefore, for in-situ AE monitoring,

Table 2 Statistical descriptions of AE characteristics

Interfacial angle /°	I-quiet period	II-developing period	III-booming period	IV-dropping period
0	There scarcely are AE signals.	The number of AE hits begins to increase, while the quantity is small and the duration is long.	The number of AE hits increases rapidly, and there is only single peak.	The number of AE hits suddenly decreases, and then scarcely appears.
15			The number of AE hits has two peaks and a drop exists between two peaks.	
30		The duration is short.	The number of AE hits has multiple peaks accompanied with multiple abrupt drops during the slip period.	
45				
60				

the possibility of rockburst hazard triggered by slip and failure of interface can be verified and evaluated based on the above AE evolutionary criteria, and the prevention measures can be early implemented.

4. Failure mechanism of combined coal-rock with different interfacial angle

The interface between coal and rock seams with different angle can be regarded as a single structural plane, which has an θ angle with the exterior normal of maximum principal plane, as shown in Fig. 11(a). There are two kinds of failure modes for combined coal-rock mass subjected to loading, which are complete failure and failure along the structural plane of sample, respectively. Assuming that the strength characteristics of structural plane meet the Mohr-Coulomb theory, according to the failure criterion of Mohr-Coulomb, the failure of structural plane needs to meet the following conditions

$$\left. \begin{aligned} \sigma &\leq R_j \text{ (or zero)} \\ \tau &\geq c_j + \sigma_j \tan \varphi_j \end{aligned} \right\} \quad (4)$$

where σ and τ are normal stress and shear stress of structural plane, and R_j , c_j , and φ_j are tensile strength, cohesion, and internal friction angle of structural plane, respectively.

The relationship curves between stress of sample and Mohr's stress circles of structural plane and coal-rock mass are shown in Fig. 11(b). From the two Mohr's stress circles, σ_{r1} is far larger

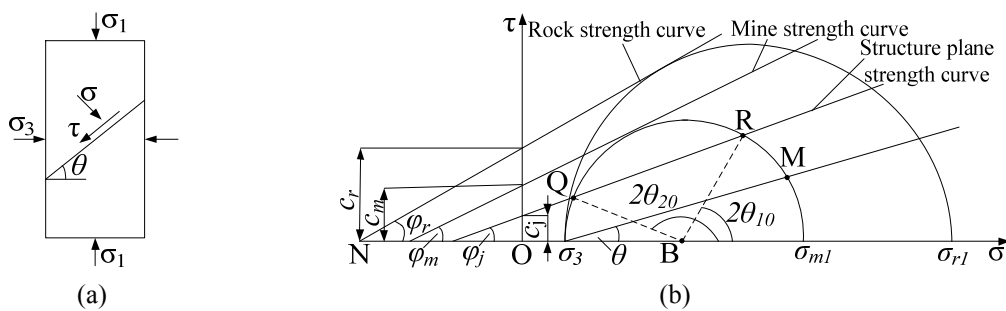


Fig. 11 Mechanical analysis of structural plane and sample failure

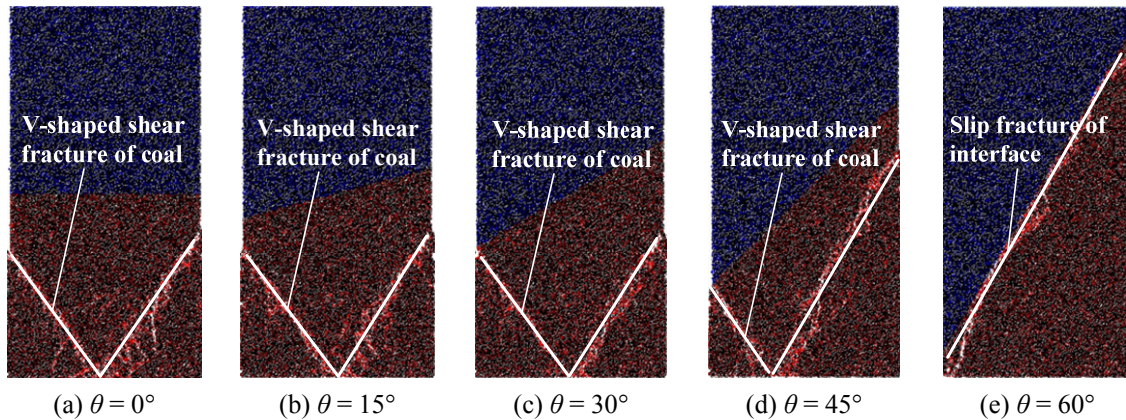


Fig. 12 Failure patterns of combined coal-rock samples under uniaxial compression

than σ_{m1} , which means that the failure of coal precedes rock mass, and thus the range of angle θ should be based on the Mohr's stress circle of coal. The failure pattern of combined coal-rock mass mainly depends on the angle θ . When 2θ is between $2\theta_{10}$ and $2\theta_{20}$, the structural plane tends to be destroyed. When 2θ is not within the scope of $2\theta_{10}$ - $2\theta_{20}$, the combined coal-rock sample tends to be completely destroyed.

4.1 Failure mechanism of combined coal-rock samples under the uniaxial compression

Fig. 12 shows the failure patterns of combined coal-rock samples with different interfacial angle under the uniaxial tests.

Fig. 12 obviously indicates that the main failure pattern is shear fracture of coal ($\sigma_3 = 0$ MPa). Since the strength curve of coal is below rock strength curve, the coal fails before rock in any case. It is shown in Fig. 11(b) that the stress point M falls between Q and R points with the increase of θ , 2θ is within the range of $2\theta_{10}$ - $2\theta_{20}$, and the failure pattern of sample will transfer from "V-shaped" shear fracture of coal to slip along fracture of the interface. With the continuous increase of θ , such sliding phenomenon becomes more and more obvious. Fig. 12(d) shows the "V-shaped" fracture of coal. Obviously, it is jointly influenced by compressive-shear stress and interfacial effect, and there is a trend that the fracture plane approaches the interface until the slip failure along the interface as shown in Fig. 12(e).

4.2 Failure mechanism of combined coal-rock samples under the biaxial compression

Fig. 13 shows four typical failure patterns of combined coal-rock samples with different interfacial angle under the biaxial tests, which are I ("V-shaped" shear fracture of coal), II (single shear fracture of coal), III (shear fracture of rock and coal), and IV (slip fracture of the interface), respectively. Test results are listed in Table 3.

According to Fig. 11(b) and Table 3, when the interfacial angles are 0° and 15° , 2θ is not within the range of $2\theta_{10}$ - $2\theta_{20}$, and thus the interface cannot be destroyed. When the interfacial angle is 30° , the slip along fracture of interface occurs along with the increase of confining stress from 1 MPa to 10 MPa, however, the failure pattern transfers into the shear fracture of coal and rock with the continuous increase of confining stress. When the interfacial angle is 45° , the failure pattern

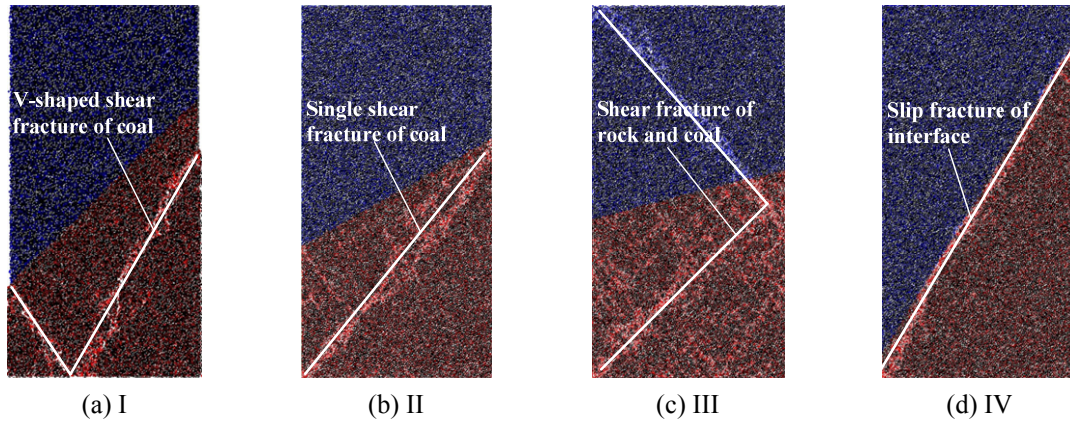


Fig. 13 Four typical failure patterns of biaxial compression tests

Table 3 Statistical results of failure patterns of biaxial compression tests

Interfacial angle/ $^{\circ}$	Confining stress/MPa						
	1	5	10	15	20	30	
0	II				III		
15	I		II			III	
30	I	II	IV		III		
45			IV			III	
60				IV			

mainly attributed to the slip along fracture of interface, and it transforms into the shear fracture of coal and rock once the confining stress reaches 20 MPa, which indicates that the confining stress can effectively constraint the slip effect of interface. When the interfacial angle is 60° , there is only slip fracture of interface because 2θ is completely within the scope of $2\theta_{10} - 2\theta_{20}$. If the confining stress is fixed, with the increase of interfacial angle, the fracture zones of coal gradually cluster near interface, and the failure pattern transforms from compressive-shear failure to slip along fracture of interface. Simultaneously, the slip effect is more and more manifest, which indicates that the failure pattern is jointly influenced by compressive-shear and interfacial slip effect. During the process of coal extraction, the bearing capacity of coal and rock mass with large dip angle far away from the excavation site is higher due to the equilibrium condition of triaxial stress which inhibits the interfacial slip effect to some extent by confining stress. However, for working faces and roadways near excavation boundary, except for the normal failure of coal and rock mass, the slip and instability failure of interface also needs to be prevented and controlled. Especially, when the interfacial angle θ is larger than 45° , the larger-scope and high-intensity slip and instability failure of coal and rock mass far away from the excavation part may occur.

In summary, when the interfacial angle θ is within $0-15^{\circ}$, the failure pattern mainly belongs to the compressive-shear failure. When the interfacial angle θ is $15-45^{\circ}$, the compressive-shear effect of combined coal-rock mass becomes weaker with the increase of interfacial angle, and the slip effect becomes stronger. When the interfacial angle θ is larger than 45° , the slip fracture dominates the failure pattern of interface. Therefore, based on the influencing degree of interfacial angle on

failure of combined coal-rock mass, the interfacial angle can be divided into three levels, which are weak-influenced scope (0-15°), moderate-influenced scope (15-45°), and strong-influenced scope (> 45°), respectively.

5. Conclusions

On the basis of the present analysis, the following conclusions are drawn:

- The uniaxial compressive strength and cohesion of combined coal-rock mass decrease with the increase of interfacial angle, while the changes of elastic modulus and internal friction angle are not obvious. The smaller the interfacial angle is, the larger the accumulated strain energy before failure is, and the faster the release velocity of strain energy is. Impact energy index K_E decreases with the increase of interfacial angle, and the failure pattern of combined coal-rock mass mainly manifests the slip and instability, which will easily trigger rockburst hazard.
- When the interfacial angle θ is larger than 15°, the number of AE hits has two peaks, which indicates the essential sign of interface slip effect. When the interfacial angle is bigger than 45°, AE fluctuates obviously and has multiple peaks during slip period. Therefore, the possibility of interface slip and instability can be predicted based on AE characteristics.
- There are four typical failure patterns of combined coal-rock mass with different interfacial angle under the biaxial tests, which are I (“V-shaped” shear fracture of coal), II (single shear fracture of coal), III (shear fracture of coal and rock), and IV (slip fracture of the interface), respectively.
- When the interfacial angle is bigger than 15°, the slip effect begins to appear and gradually enhance with the increase of interfacial angle, while the confining stress can effectively inhibit the slip effect. According to the influencing degree of interfacial angle on combined coal-rock mass failure, the angle can be divided into 3 levels, which are weak-influenced scope (0-15°), moderate-influenced scope (15-45°), and strong-influenced scope (> 45°), respectively.

Acknowledgments

The research described in this paper was financially supported by Natural Science Foundation of China (51474136), the Open Research Program of Key Laboratory of Safety and High-efficiency Coal Mining, Ministry of Education (Anhui University of Science and Technology) (JYBSYS2014202, JYBSYS2014203), and the Foundation for the Author of National Excellent Doctoral Dissertation of P.R. China (201167).

References

- Bell, F.G. (2000), *Engineering Properties of Soils and Rocks*, (4th Edition), Butterworth-Heinemann, Oxford, UK, 482 p.
- Brady, B.H.G. and Brown, E.T. (1993), *Rock Mechanics for Underground Coal Mining*, (2nd Edition), George Allen and Unwin, London, UK, 571 p.
- Chen, X., Liao, Z.H. and Peng, X. (2012), “Deformability characteristics of jointed rock masses under

- uniaxial compression”, *Int. J. Mining Sci. Technol.*, **22**(2), 213-221.
- Inmaculada Alvarez-Fernandez, M., Amor-Herrera, E., Gonzalez-Nicieza, C., Lopez-Gayarre, F. and Rodriguez Avial-Llardenet, M. (2013), “Forensic analysis of the instability of a large-scale slope in a coal mining operation”, *Eng. Fail. Anal.*, **33**, 197-211.
- Guo, D.M., Zuo, J.P., Zhang, Y. and Yang, R.S. (2011), “Research on strength and failure mechanism of deep coal-rock combination bodies of different inclined angles”, *Rock Soil Mech.*, **32**(5), 1333-1339. [In Chinese]
- Lu, C.P., Liu, G.J., Liu, Y., Zhang, N., Xue, J.H. and Zhang, L. (2015), “Microseismic multi-parameter characteristics of rockburst hazard induced by hard roof fall and high stress concentration”, *Int. J. Rock Mech. Min. Sci.*, **76**, 18-32.
- Mishra, B. and Verma, P. (2015), “Uniaxial and triaxial single and multistage creep tests on coal-measure shale rocks”, *Int. J. Coal Geol.*, **137**, 55-65.
- Mohtarami, E., Jafari, A. and Amini, M. (2014), “Stability analysis of slopes against combined circular-toppling failure”, *Int. J. Rock Mech. Min. Sci.*, **67**, 43-56.
- Petukhov, I.M. and Linkov, A.M. (1979), “The theory of post-failure deformations and the problem of stability in rock mechanics”, *Int. J. Rock Mech. Min. Sci.*, **16**(2), 57-76.
- Poulsen, B.A., Shen, B., Williams, D.J., Huddleston-Holmes, C., Erarslan, N. and Qin, J. (2014), “Strength reduction on saturation of coal and coal measures rocks with implications for coal pillar strength”, *Int. J. Rock Mech. Min. Sci.*, **71**, 41-52.
- Tan, Y.L., Li, F.C. and Zhou, H. (2000), “Analysis on acoustic emission pattern for rock burst”, *Chinese J. Rock Mech. Eng.*, **19**(4), 425-428. [In Chinese]
- Tan, Y.L., Zang, Z. and Zhao, T.B. (2011), “AE pattern of rock burst disaster induced by strata activation in coal mine”, *Disaster Adv.*, **4**(4), 29-33.
- Tan, Y.L., Yin, Y.C. and Gu, S.T. (2015), “Multi-index monitoring and evaluation on rock burst in Yangcheng Mine”, *Shock Vib.*, Article ID 624893.
- Thomas, L. (2002), *Coal Geology*, John Wiley and Sons, New York, NY, USA, 384 p.
- Vakili, A. and Hebblewhite, B.K. (2010), “A new cavability assessment criterion for longwall top coal caving”, *Int. J. Rock Mech. Min. Sci.*, **47**(8), 1317-1329.
- Ward, C.R. (1984), *Coal Geology and Coal Technology*, Blackwell Scientific Publications, Melbourne, Australia, 345 p.
- Yin, Y.C., Zhao, T.B. and Tan, Y.L. (2015), “Reconstruction and numerical test of the mesoscopic model of rockbased on Otsu digital image processing”, *Rock Soil Mech.*, **36**(9), 2532-2540.
- Zhao, Z.H., Wang, W.M., Wang, L.H. and Dai, C.Q. (2015a), “Compressive-shear strength criterion of coal-rock combination model considering interface effect”, *Tunn. Undergr. Sp. Tech.*, **47**, 193-199.
- Zhao, T.B., Yin, Y.C., Tan, Y.L. and Song, Y.M. (2015b), “Deformation tests and failure process analysis of an anchorage structure”, *Int. J. Min. Sci. Technol.*, **25**(2), 237-242.
- Zuo, J.P., Wang, Z.F., Zhou, H.W., Pei, J.L. and Liu, J.F. (2013), “Failure behavior of a rock-coal-rock combined body with a weak coal interlary”, *Int. J. Min. Sci. Technol.*, **23**(6), 907-912.